Stability analysis of steel compression members under shock loads

ANETA BRZUZY, GRZEGORZ BĄK

Military University of Technology, Faculty of Civil Engineering and Geodesy,
2 Gen. W. Urbanowicza Str., 00-908 Warsaw, Poland,
aneta.brzuzy@wat.edu.pl, grzegorz.bak@wat.edu.pl

Abstract. This paper presents the results of a numerical analysis of the elastic-plastic behaviour of steel compression members subjected to compression with a permanent pre-deformation in the longitudinal axis by a longitudinal indispensable shock load. A differential load intensity was considered up to the loss of stability. A finite difference method was applied, with an explicit integration schema for the time of the dynamic stability equations. It was assumed that the precursor to the unstable behaviour of a steel compression member was a continuous deformation of the rod axis, which was defined according to current industry-standard design procedures. Cases of flexible and stiff rods, varying in slenderness, were considered. It was demonstrated that a significant load on the performance of the steel compression members and their buckling mechanisms is attributable to longitudinal wave effects. These longitudinal wave effects cause high-frequency changes in the axial forces with a significant stress concentration due to the effect of reflection from a pinned support. This is critical for the dissipation of internal energy by plastic deformation. The applied research method facilitated an estimation of the dynamic critical forces and their relationships with static values.
Keywords: steel rods with pre-deformation of axis, elastic-plastic behaviour, dynamic stability of rods, differential approximation, effects of axial wave response
DOI: 10.5604/01.3001.0011.8051

1. Introduction

The dynamic stability of rods is a problem widely covered in the reference literature. Examples of this include monographs [1] and [2]. The loss of stability of a straight rod with a pivot support under a shock load $P(t) = $ const was studied in [3]. The analysis was based on an elastic dynamic equation derived without consideration of the stiffening principle. The analysis did not consider axial vibration

or the risk of plastification in the cross-sections. [4] was a study of an inelastic behaviour of square beams and H-beams subjected to high-intensity transverse shock loads. The loads initiated elastic-plastic behaviour, exhibited by moderately high deflections. The behaviour of the beams was tested with the simultaneous application of a longitudinal boundary force of varying intensity. The described behaviour of the beams included longitudinal vibration. The values of the longitudinal force, which triggered unlimited displacement, were determined. This reference can be understood as testing the stability of eccentrically-compressed steel rods.

This work considered the problem of the dynamic behaviour of compressed steel rods which feature a circular-tubular cross-section. The steel rods were exposed to impact loads which could have resulted in buckling of the former. A longitudinal compressive force applied to a steel rod retained its intensity, sense and direction of action over a long time frame. This type of load could be qualified in the category of exceptional loads, a major object of focus in modern structural design standards [5].

The loss of stability of a steel rod depends on Euler's limit of slenderness. Under these conditions, elastic and non-elastic buckling cases are studied, in which the steel rods are defined as flexible steel rods and stiff steel rods. In the cases of dynamic shock loads, this definition of the steel rods should not be applied to determine the nature of buckling. Under a longitudinal boundary force with a steady intensity, a steel rod may suffer elastic-plastic deformation. If the elastic-plastic deformation is not increased without any limit, the steel rod should be deemed to be conforming to the load applied to it. The loss of stability is always concomitant to an avalanche process of inelastic failures, which is an unlimited increase in the plastic deformation, resulting in an uninhibited dissipation of internal energy. It would be interesting to estimate the value of the dynamic critical force at which the destructive effects of buckling occur. The destructive effects of buckling are always preceded by an initial phase, which may fail to change into the uninhibited failure phase if explosive decaying loads are present. A determination of the initial phase duration may provide useful data for the design of structural components exposed to short explosive loads.

This paper presents the solutions of the problems of the dynamic behaviour of a steel rod loaded with a longitudinal boundary force, with the assumption that the steel rod has an initial sine-form camber. The sense of this camber is a corresponding fractional length of the steel rod. It was assumed by the authors that the initial sine-form camber provides a more accurate representation of real-life cases and could reflect a continuous geometric imperfection caused by manufacturing processing of the steel rod, and a certain random eccentricity of the application of the compressive force [6].

In this work, the longitudinal wave behaviour of steel rods was considered without transverse loads and with preset geometrical imperfections along the longitudinal axis. It was assumed that the stock material of a steel rod has an ideal elastic-plastic behaviour. The effect of the propagation of longitudinal waves was considered with their interaction with transverse vibration, generated by a dynamic loss of stability.

The dynamic longitudinal displacement and deflections were assumed to be small and interposed on the initial deformation, which required dynamic balance equations defined under the moderately high deflection theory. The system of dynamic balance equations included the preset initial deformation of the steel rod; the description of the load states did not include indeterminate internal stresses.

2. Basic equations

The static diagram and the load on the steel rod are shown in Fig. 1. To assume the method for discretization of the steel rod, the axial load $P(t)$ was assumed to be applied to the boundary mass m_A. The initial deformation of the axis of the steel rod were input as follows:

$$w_0(x,0) = w_0 \sin \frac{k\pi x}{H} \tag{1}$$
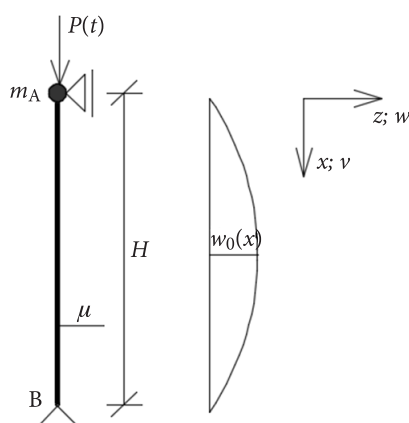
with: $k = 1, 2,...$

Fig. 1. Static diagram of a compressed steel rod and the form of its initial axis deformation at $k = 1$.

The amplitude of initial deflection was assumed according to the generalized imperfections defined in [1];

$$w_0 = \frac{H}{M}, M = 500, 250, 200, 150. \tag{2}$$

This deformation of the axis of the steel rod initiated a destabilization behaviour in the steel rod, which could in turn initiate the process of stability loss.

The analysis discussed here was carried out with a system of equations specific to low dynamic longitudinal displacements $v(x, t)$ and moderately high dynamic

deflections $w(x, t)$. The moderately high dynamic deflections were superposed on the preliminary imperfections in the description of the geometrical changes:

$$\frac{\partial}{\partial x}\left[Q + S\left(\frac{\partial w_0}{\partial x} + \frac{\partial w}{\partial x}\right)\right] - \mu\frac{\partial^2 w}{\partial t^2} = 0,$$

$$Q = \frac{\partial M}{\partial x}, \tag{3}$$

$$\frac{\partial S}{\partial x} - \mu\frac{\partial^2 v}{\partial t^2} = 0.$$

The values of $Q(x, t)$, $M(x, t)$ and $S(x, t)$ were the internal forces in the deformed steel rod; $\mu = \rho * A$ — unit mass of the steel rod with cross-section A, ρ — specific density of steel.

Note that the equation $(3)_1$ features the forces of inertia being a consequence of the dynamic deflection $w(x, t)$ only, which was measured along the axis of the deformed steel rod. The forces of longitudinal inertia were approached in an analogous manner, and the equation $(3)_3$ could be transformed to accentuate the propagation of a longitudinal wave,

$$\frac{\partial^2 v}{\partial x^2} - a\frac{\partial^2 v}{\partial t^2} = 0 \tag{4}$$

with $a = \sqrt{\dfrac{E}{\rho}}$ being the velocity of the longitudinal wave in elastic deformation. This form was not used, given that this work considered plastic deformation. The dynamic boundary conditions resulted from the conditions of the bearing of the steel rod and the boundary effect:

$$M(0,t) = 0, \qquad M(H,t) = 0.$$

$$S(0,t)\cos\alpha(0) + Q(0,t)\sin\alpha(0) - m_A\left.\frac{\partial^2 v}{\partial t^2}\right|_{x=0} = P(t) \tag{5}$$

with angle $\alpha_0 \approx \left.\dfrac{\partial(w_0 + w)}{\partial x}\right]_{(x=0,t)}$. For the investigated deflections of the value $\cos\alpha(0) \approx 1$, whereas $\sin\alpha(0) \approx \alpha(0)$. $P(t)$ was the force of constant direction, $P(t) = P_0...$for$....t \geq 0$. The solution of the system of equations (3) required reducing the system to a displacement form. This was done by applying the geometrical relationships with the dynamic deformations, the longitudinal strain of the axis of the steel rod $v(x, t)$ and the steel rod's curvature $\kappa(x, t)$ associated with the dynamic deflection $w(x, t)$,

$$e(x,t) = \frac{\partial v}{\partial x} \qquad \kappa(x,t) = -\frac{\partial^2 w}{\partial x^2}. \tag{6}$$

If the state of load of the cross-section existed in an elastic range, the following relations applied:

$$S(x,t) = EA * e(x,t), \quad M(x,t) = EJ * \kappa(x,t) \tag{7}$$

The internal forces in the elastic-plastic range were determined appropriately for the values of the deformation resulting from the flat cross-section assumed here.

$$\varepsilon(x,z,t) = e(x,t) + \kappa(x,t) * z. \tag{8}$$

The distribution of stresses in the cross-sections were integrated by layered discretization of the cross-sections.

3. The discrete model of the steel rod and difference equation

The numerical solutions to the problems of dynamic inelastic behaviour of the steel rod were achieved by applying the discrete model shown in Fig. 2(a). The circular-tubular cross-section of the steel rod was replaced with a system of 14 layers with different cross-sections, based on inner diameter d_w and outer diameter d_z.

The discrete model of the steel rod was determined according to the general principles for construction of discrete models of longitudinal wave propagation
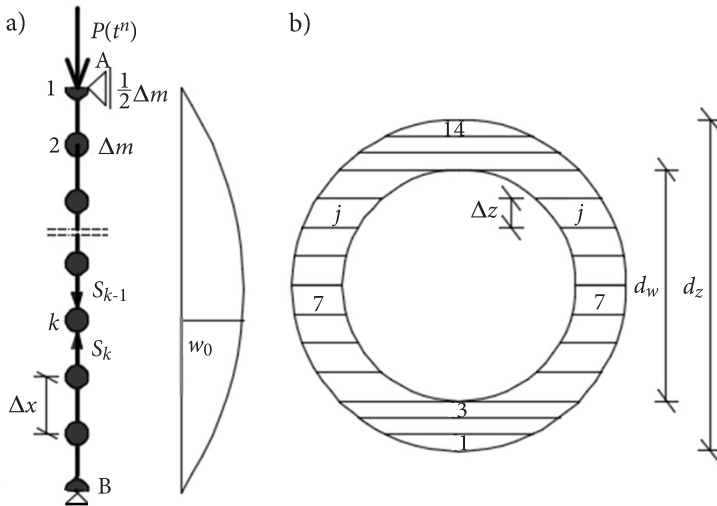

Fig. 2. Spatial discretization of the steel rod: (a) the system of focused masses along the steel rod compressed with a schematic initial deflection; (b) the discretization of the cross-section of the steel rod, with the layers numbered.

in rods [7]. The principles comprise the division of the steel rod into nodes with discrete masses, interlinked with deformable straight sections. A valid description of longitudinal wave behaviour required forming the initial half mass $m_A = \frac{1}{2}\Delta m$ from a boundary part of the steel rod. This provided the required formation of the wave penetrating the steel rod from the application of an external load, and the wave reflected from the same support as a free boundary and caused by the generated wave being a wave reflected from pinned support B and reaching roller support A. The effects of longitudinal deformation were attributed to the deformable straight sections, whereas the effects of elastic deformation were the transverse displacements attributed to the focused masses of the discrete model. A proof of the stresses was then carried out at a cross-section of the focused mass where the bending moment was known. The longitudinal force $S_{k-0.5}(t)$ associated with the bending moment was determined by introducing a correction of the sectional value of $S_k(t)$ according to the formula below:

$$S_{k-0,5}(t) = S_k(t) + \frac{1}{2}\Delta m \ddot{v}_k. \tag{9}$$

The propagation of the wave penetrating the steel rod by the action of the external boundary load $P(t)$ required a singular temporal discretization of that load's action [8] by using the formula:

$$P(t^n) = \begin{Bmatrix} 0,5P(0),... \, n = 1 \\ \bar{P}_{SREDNIE}(t^{n-1,n}), \quad \text{when...} \, n > 1 \end{Bmatrix} \equiv P_0. \tag{10}$$

The longitudinal vibrations were determined by simultaneously mapping the transverse vibrations caused by the initial imperfection, a destabilization factor of the steel rod's behaviour.

The cases contemplated here did not permit an error-free differential approximation [8]. Hence it was necessary to investigate the stability of numeric procedures and the convergence of solutions.

The essential components of a computer program designed to determine the acceleration values at the start of a time step t^n were:

$$\ddot{v}_k^n = \frac{1}{\Delta m}(S_{k+1} - S_k), \quad \ddot{w}_k^n = \frac{\Delta^2 M}{\Delta x^2} + S\frac{\Delta^2 w}{\Delta x^2} + \Delta S\frac{\Delta w}{\Delta x}\bigg|_k^n. \tag{11}$$

The increments of displacements and the displacements at the end of the same time step were determined as follows.

$$\Delta v_k^{n,n+1} = \Delta v_k^{n-1,n} + \ddot{v}_k^n * \Delta t, \quad \Delta w_k^{n,n+1} = \Delta w_k^{n-1,n} + \ddot{w}_k^n * \Delta t,$$
$$v_k^{n+1} = v_k^n + \Delta v_k^{n,n+1}, \quad w_k^{n+1} = w_k^n + \Delta w_k^{n,n+1}. \tag{12}$$

Based on these results, the deformation at the start of the time step t^{n+1} were determined for cross-sectional layer j of the steel rod located at node k, pursuant to the assumption of the cross-section being flat (8),

$$\varepsilon_{k,j}^{n+1} = e_k^{n+1} + \kappa_k^{n+1} * z(j). \tag{13}$$

With the known deformations in the cross-sectional layers until the time t^{n+1} inclusive, it was possible to determine the deformations according to the adopted physical model of the steel rod's material. Based on the integral summation definitions of the internal forces, the active internal forces S_k^n and M_k^n in the compressed steel rod were determined, and based on (3)$_2$, the passive force Q_k^n was determined.

This procedure facilitated an analysis of the behaviour of a steel rod subjected to a shock load which induced a dynamic and high-frequency process dominated by compression. The process originated from the behaviour of the eccentrically compressed steel rod within the limits of elastic or elastic-plastic deformations, and initially without any manifestation of instability effects. At a high intensity of applied compressive force, symptoms of stability loss could appear as avalanche-intensified elastic-plastic deformations, i.e. the unlimited dissipation of internal energy.

4. Analytical program and numerical results illustrating a dynamic behaviour with loss of stability of the steel rods

The behaviour of three steel rods was investigated. The steel rods were made of S235 grade steel and had the form of round tubes with inner diameter $\varphi = 101.6$ mm, wall thickness $g = 8.8$ mm and cross-section A = 0.00257 m². Euler's limit of slenderness of the steel rods was $l_{gr} = 96$. The compressed steel rods were assumed to feature simple support conditions, with the flexibility determined by the varying length, respectively: $H_1 = 5.40$ m, $H_2 = 3.60$ m, and $H_3 = 2.80$ m. The slenderness values of the steel rods were: $l_1 = 164 > l_{gr}$, $l_2 = 109 > l_{gr}$ and $\lambda = 84.8 < l_{gr}$. The values of the static critical forces, determined with Euler's formula for flexible steel rods "1" and "2", and Tetmajer-Jasiński's formula for steel rod "3" were:

$$P_{CR}^{(1)} = 194,5 \text{ kN}, \quad P_{CR}^{(2)} = 437,6 \text{ kN}, \quad P_{CR}^{(3)} = 565,5 \text{ kN}.$$

Each of the steel rods had an axial imperfection resulting from $M = 200$ in the formula (2). The discretization of the axes of the steel rods featured 14 sections with $\Delta x \approx 0.17$ m. The intensity of the dynamic longitudinal shock load was analysed at values related to the static critical forces, where $P(t) = P_0 = \eta P_{CR}^{(1)} = \text{const}$.

The longitudinal deformations of the steel rods' axes were caused by the propagation of a longitudinal wave plus the effects of reflection from the steel rod's boundaries, the pinned support, and the roller support, which was the end point of the steel rod.

The longitudinal forces, which varied along the steel rods, caused a moment behaviour in the cross-sections with an initial deformation defined in (2).

The illustration of the results of numerical analysis for an extremely flexible steel rod is shown in Figs. 3, 4 and 5.

Figs. 3 and 4 show the behaviour of the steel rod which did not suffer buckling and with varying plastic deformations caused by transverse vibration of the steel rod.

The results of the numerical analysis presented here indicated that the values of dynamic shock force, which were slightly below the static critical force and 16% above the value, caused the steel rod to behave like an eccentrically compressed element within the limits of elastic-plastic deformation caused by transverse and longitudinal vibrations. This behaviour was dominated by a bending deformation mechanism. This was partial to a temporal change in the dynamic deflection of the centre of the steel rod. (Fig 3 a). There was a certain dynamic axial displacement of the end of the steel rod. These phenomena were caused by the permanent longitudinal effects generated within the zone at the pinned support, mostly due to wave reflections. The permanent deformations determined the nature of elastic vibration in the first section of the discrete model.

An analogous characterization of the behaviour of the extremely flexible steel rod applied during exposure to a shock force $P_0 = \eta^* P_{cr} = 225.6$ kN, $\eta = 1.16$. The lack of stability loss of the steel rod at the values analysed here was demonstrated by the stabilisation of energy dissipation which followed relatively long time periods, expressed by the multiplicity of the basic period T_0 determined for the steel rod represented by a deflected beam. The periods could be qualified as the period of adaptation of the steel rods to the action of the applied dynamic load.

The stability of the steel rod was lost at a dynamic compressive force 20% above the static critical force. The dynamic character of the loss of stability of the steel rod was illustrated by the avalanche increment of the deflection in the centre of the steel rod, see Fig. 5.

Figs. 6, 7 and 8 show the numerical analysis results for a case of a flexible steel rod exposed to dynamic forces defined by $\eta_2 = 0.5$ and $\eta_2 = 0.8$. The steel rod demonstrated a stable behaviour following the emergence of elastic-plastic deformations. The energy dissipation by plastic deformation was located mainly based on the deflection behaviour of the steel rod, i.e. the significant deflection of its middle cross-section. The dynamic deflections of the steel rod in the presence of longitudinal forces result in the formation of plastification zones in the middle section. Figs. 6(a) and 7(a) illustrate the emergence of permanent dynamic deformation of the axis of the steel rod. The assumed deformation model of the ideally elastic-plastic material and the high intensity of the shock load caused permanent deflections, around which non-attenuated transverse vibrations were found. These were secondary elastic vibrations. The vibrations died away after the initial period, which was equal to approx. $1600 \times T_0$ in both cases. Moreover, the steel rod suffered an energy dissipation caused
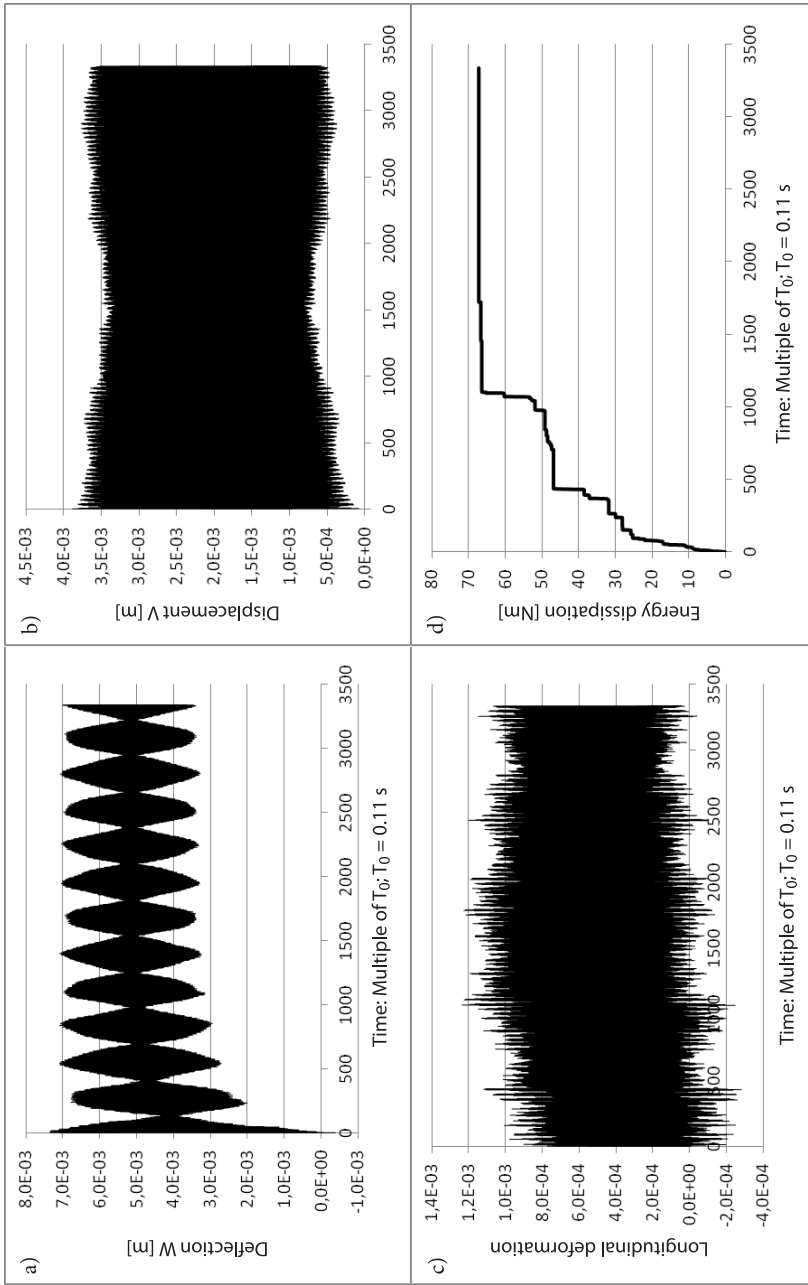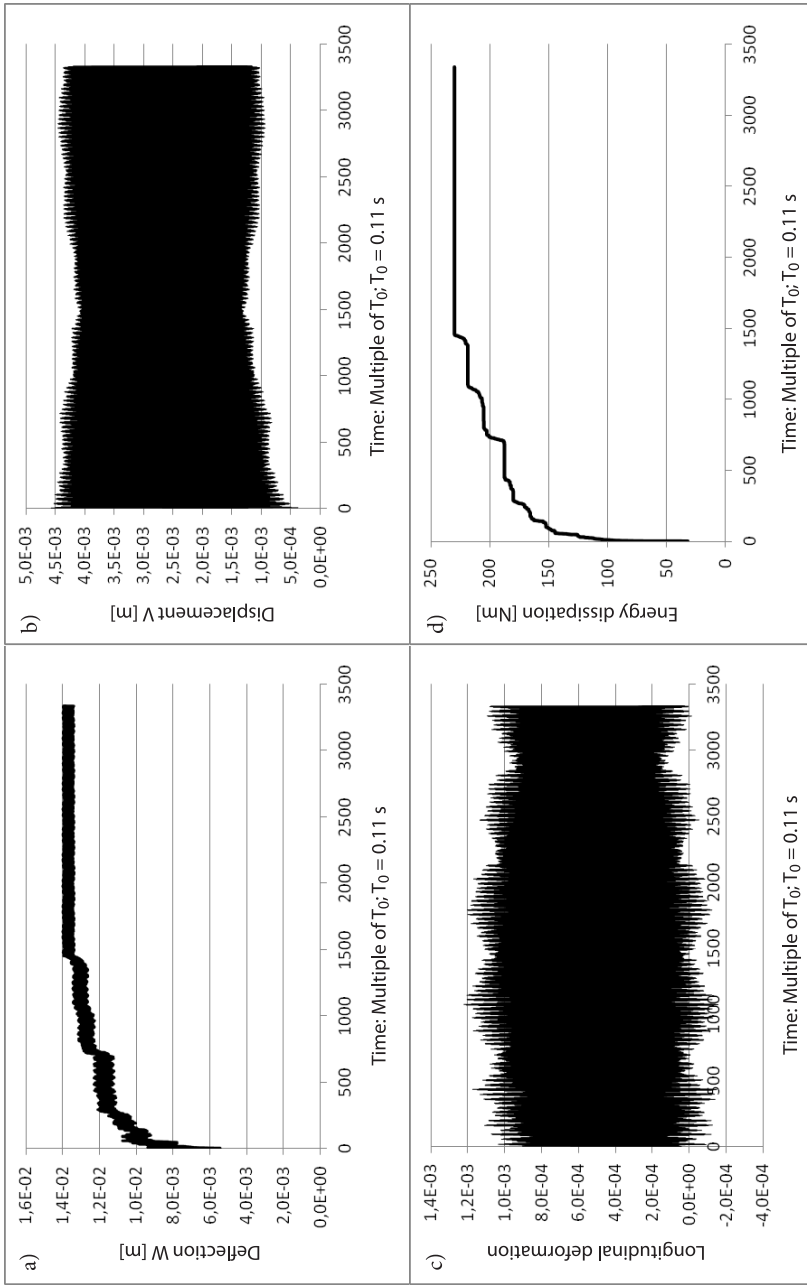
Fig. 3. Steel rod, length $H = 5.4$ m; slenderness $l = 164$; $P_{cr} = 194.5$ kN; $\eta = 0.98$; $P_s = \eta \cdot P_{cr} = 190.6$ kN: (a) dynamic deflection of the centre of the steel rod, permanent dynamic deformation by 5.3 mm; (b) dynamic longitudinal displacement of node 1, permanent dynamic displacement by 2.1 mm; (c) dynamic longitudinal axial deformation of support-interfaced node 18, permanent deformation by 0.54‰; (d) evolution of energy dissipation, decay of increment after $1700 \times T_0$.

Fig. 4. Steel rod, length $H = 5.4$ m; slenderness $l = 164$; $P_{cr} = 194.5$ kN; $\eta = 1.16$; $P_s = \eta * P_{cr} = 225.6$ kN: (a) dynamic deflection of the centre of the steel rod, permanent dynamic deformation by 1.35 cm; (b) dynamic longitudinal displacement of node 1, permanent dynamic displacement by 2.65 mm; (c) dynamic longitudinal axial deformation of support-interfaced node 18, permanent deformation by 0.5‰; (d) evolution of energy dissipation, decay of increment after $1500 \times T_0$.
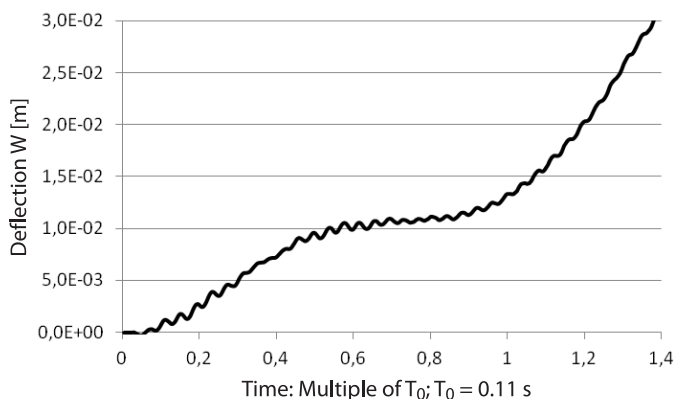
Fig. 5. Dynamic deflection of the centre of the steel rod with length $H = 5.4$ m at $P_s = \eta^* P_{cr} = 233.4$ kN, $\eta = 1.2$, $P_{cr} = 194.5$ kN.

by the effects of the reflection of the wave of axial stresses, which occurred along the section adjacent to the pinned support, see Figs. 6(c) and 7(c). A consequence of the plastic deformation in this location was the longitudinal displacement of the end of the steel rod, see Figs. 6(b) and 7(b). The displacements were not elastic-plastic; they were elastic only. The permanent displacement as suggested in the figures was not caused by inelastic deformations in the first section of the discrete model, but by the plastification of the sections located at the bottom pinned support, where the effects of reflection of the longitudinal wave were cumulative.

The temporal profiles of variations in the energy dissipation are shown in Figs. 6(d) and 7(d). The energy dissipation process ended after approximately $2700 \times T_0$. This would seem to be partial to the evolution of a long-term longitudinal deformation process of the section adjacent to the pinned support. Expressed in units of time, the period of this process was approximately 130 s.

The result being the estimate of the period was a consequence of the theoretical assumptions of the numerical analysis. The propagation of the axial wave considered in the computer program was not attenuated, i.e. there was no decay in the discontinuity of the reflections generated by the effects. Consequently, an ideally elastic-plastic model of the material was applied with a definition typical of wave mechanics. The longitudinal waves did not generate any transverse waves; they did, however, cause cumulative increments in the plastic deformations within the area of the pinned support. The diagram of the support did not reflect its capacity for absorption of the energy of the longitudinal waves. Hence, the support only generated the effects of reflections.

The loss of stability was caused by a dynamic force at an intensity of $\eta_2 = 0.9$, as shown in Fig. 8. The figure shows that the avalanche increase in the dynamic deflection began after the period of initial vibrations, which featured acceptable
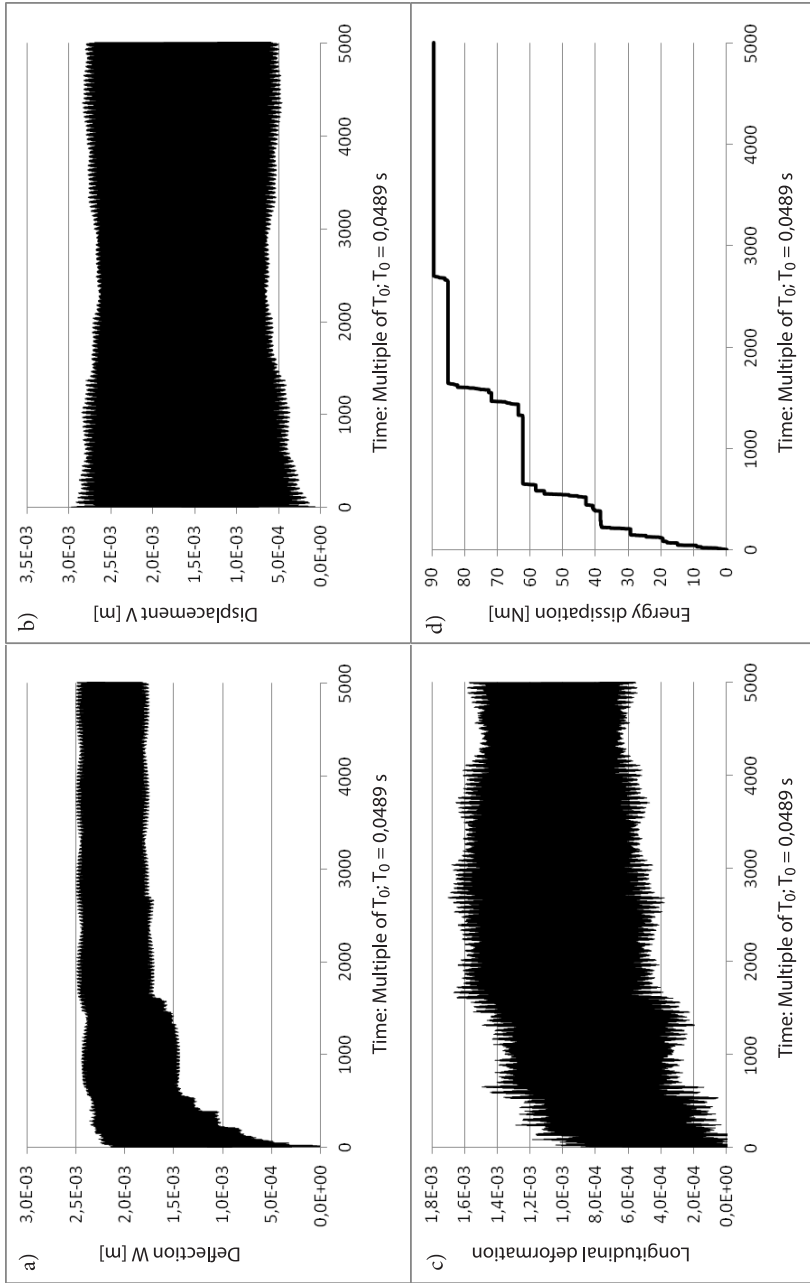
Fig. 6. Steel rod, length $H = 3.6$ m; slenderness $l = 109$; $P_{cr} = 437.6$ kN; $\eta = 0.5$; $P = \eta * P_{cr} = 218.8$ kN: (a) dynamic deflection of the centre of the steel rod, transverse vibration stabilized after 1640 T_0, permanent dynamic deformation by 2 mm; (b) dynamic longitudinal displacement of node 1, permanent dynamic displacement by 1.8 mm; (c) dynamic longitudinal axial deformation of support-interfaced node 18, permanent deformation by 1.1‰; (d) evolution of energy dissipation, decay of increment after 2700 × T_0.
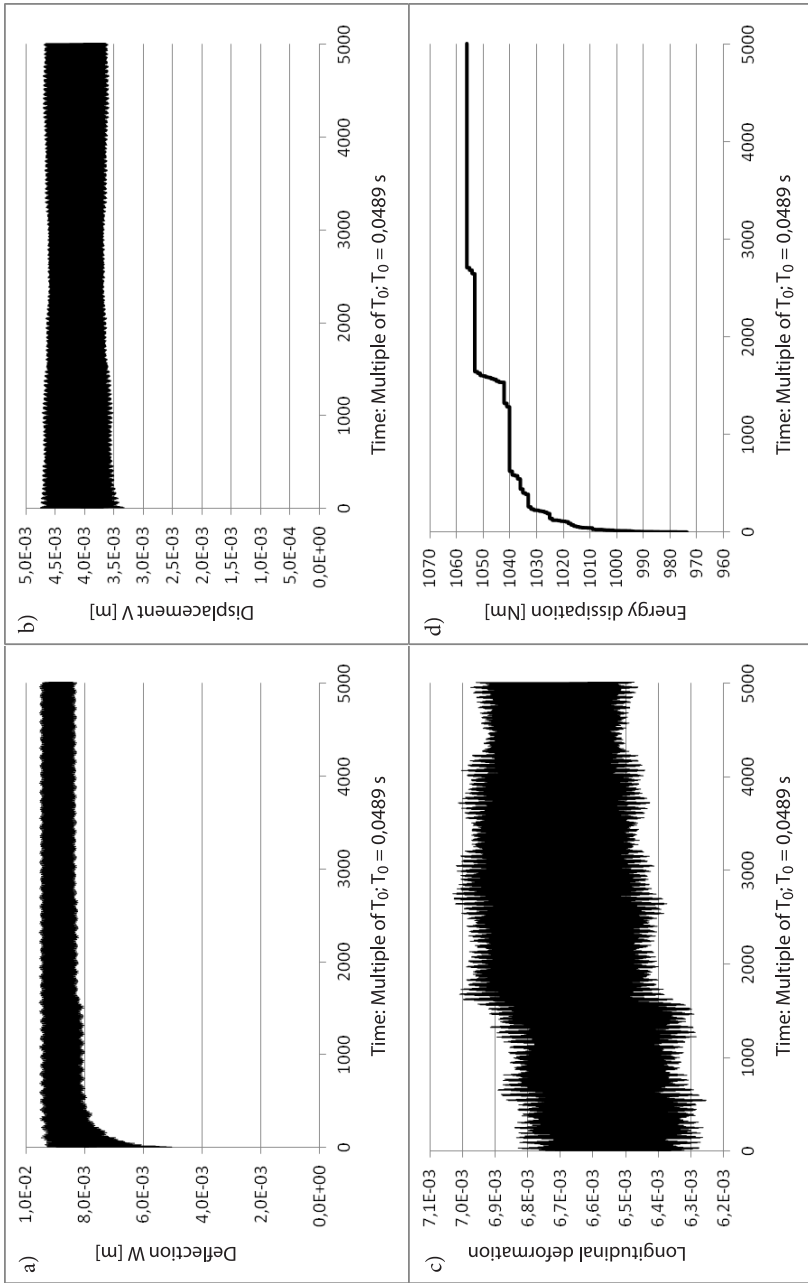
Fig. 7. Steel rod, length $H = 3.6$ m; slenderness $l = 109$; $P_{cr} = 437.6$ kN; $\eta = 0.8$; $P_s = \eta^* P_{cr} = 350.08$ kN: (a) dynamic deflection of the centre of the steel rod, transverse vibration stabilized after 1600 T_0, permanent dynamic deformation by 9 mm; (b) dynamic longitudinal displacement of node 1, permanent dynamic displacement by 4 mm; (c) dynamic longitudinal axial deformation of support-interfaced node 18, permanent deformation by 6.7‰; (d) evolution of energy dissipation, decay of increment after approx. $2700 \times T_0$.
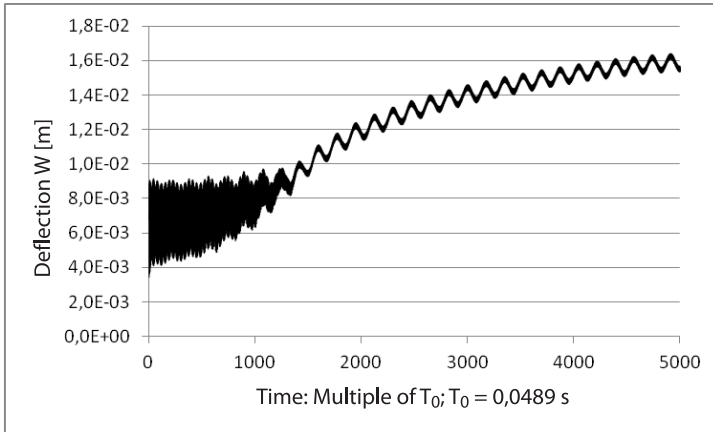
Fig. 8. Dynamic deflection of the centre of the steel rod with a length $H = 3.6$ m at the dynamic force $P_0 = \eta * P_{cr} = 393.8$ kN, $\eta = 0.9$.

deformations. That period was estimated to be $1200 \times T_0$ long, i.e. approximately 58 s. This large deceleration of the effects of avalanche stability loss was caused by the previously discussed singularities in the analysis of the longitudinal waves. Omitting the wave analysis would result in a longitudinal force at a constant value of P_0 along the entire steel rod. Inclusion of the effects of propagation of the waves reduced the effect of destabilization of the steel rod. The effects of longitudinal waves were cumulative mostly at the bottom pinned support. The central part of the steel rod revealed significant transient discharges, with very short transient tensions. This would explain the duration before the avalanche stability loss.

Figs. 9 and 10 illustrate the behaviour of a stiff steel rod, length $H = 2.80$ m exposed to a shock load at the critical intensity $P_{cr} = \eta_{cr} P_{crTJ}$, at $\eta = 0.5$ and $\eta = 0.75$. Note the general conclusion drawn from the analyses of the problems of stability of the steel compression members contemplated here as exposed to static loads. There is no indication that deflection failure mechanisms would evolve; plastification states were only reached in the cross-sections under eccentric compression; see the concepts by Tetmajer-Jasiński or Johnson-Ostenfelf [9]. It would be natural for a dynamic analysis that stiff steel rods would not feature a typical mechanism of stability loss, but the limit state, due to the excessive longitudinal plastic deformations concentrated at the pinned support. The discovered deflection of the steel rod were not intensified, which was confirmed by the missing beam failure mechanism typical of flexible rods. The figures illustrate the initial periods of behaviour of the steel rod without any symptoms of loss of stability; the only symptoms found included a significant load in plastic deformations. The effort was caused by the emergence of significant axial deformations in the lower sections of the discrete model. The axial deformations this high, and expressed as percentage
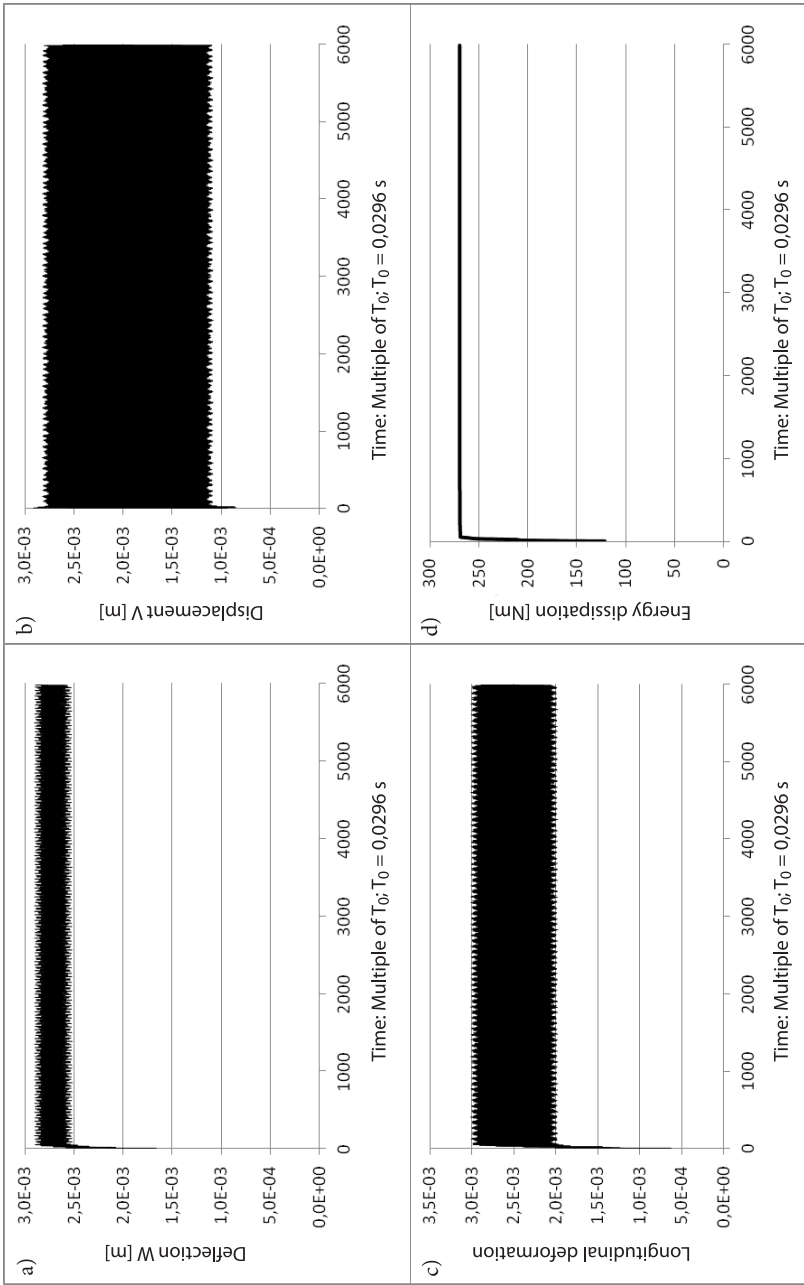
Fig. 9. Steel rod, length $H = 2.8$ m; slenderness $l = 85$; $P_{cr} = 565.5$ kN; $\eta = 0.5$; $P_s = \eta^* P_{cr} = 282.75$ kN: (a) dynamic deflection of the centre of the steel rod, permanent dynamic deformation by 2.7 mm; (b) dynamic longitudinal displacement of node 1, permanent dynamic displacement by 1.65 mm; (c) dynamic longitudinal axial deformation of support-interfaced node 18, permanent deformation by 2.5‰; and (d) evolution of energy dissipation, decay of increment after $55 \times T_0$.
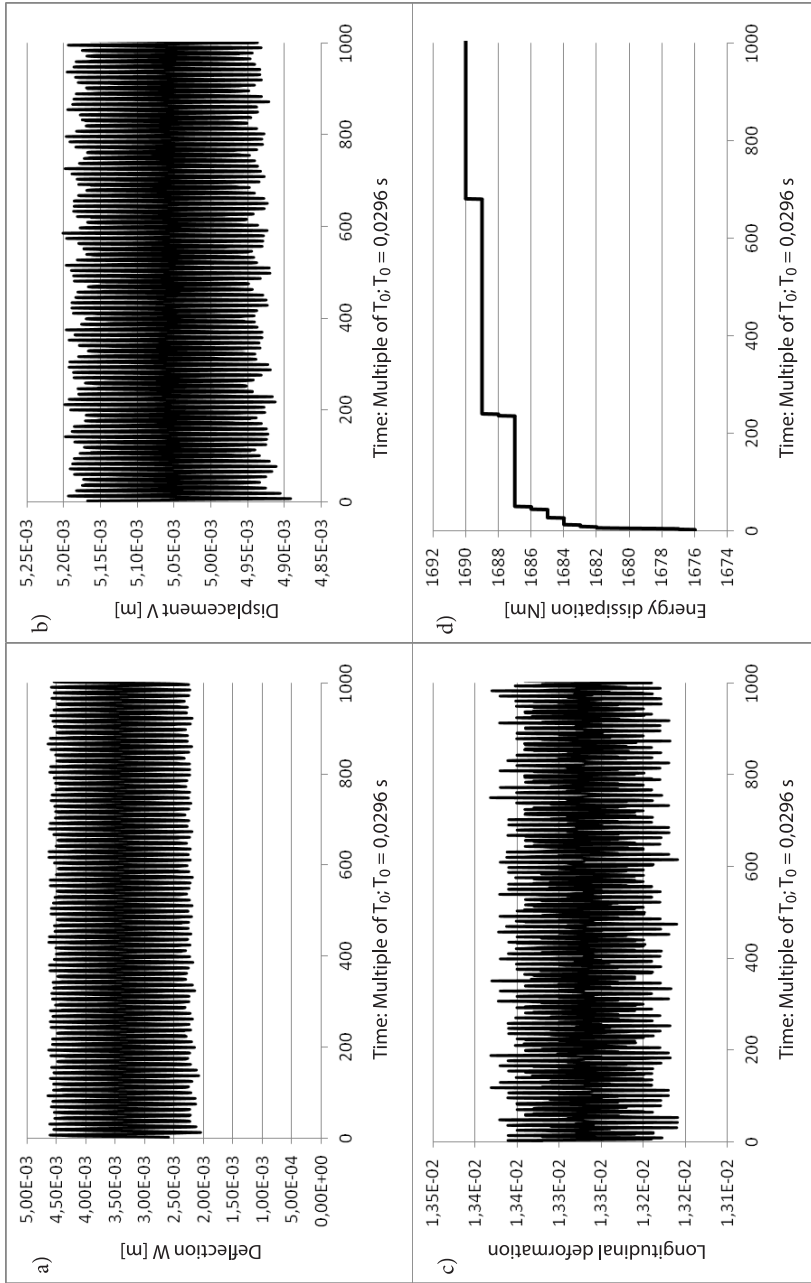
Fig. 10. Steel rod, length $H = 2.8$ m; slenderness $l = 85$; $P_{cr} = 565.5$kN; $\eta = 0.75$; $P_s = \eta^*P_{cr} = 424.1$ kN: (a) dynamic deflection of the centre of the steel rod, permanent dynamic deformation by 3.4 mm; (b) dynamic longitudinal displacement of node 1, permanent dynamic displacement by 5.1 mm; (c) dynamic longitudinal axial deformation of support-interfaced node 18, permanent deformation by 13.3‰; and (d) evolution of energy dissipation, decay of increment after $680 \times T_0$. No stability loss was shown due to the high longitudinal deformation v; the force of 424.1 kN could be qualified as critical.

values, necessitated analysis according to the theory of high deformation, and a due consideration of the localized effects of instability in tubular steel rods, i.e. the instability of the rod wall. For the given steel rods, it would be possible to analyse this at much higher loads, exceeding the static critical force. No results were presented due to their unreliability. The applied theory of definition was adopted in this paper for low deformation values, which resulted in high deformation values.

5. Conclusions

The numerical analyses based on a conditionally stable difference method demonstrated that the cases of the flexible steel rod and the stiff steel rod necessitated the application of varying values of the time steps for equation integration over time. The definition of behaviour of the flexible steel rod was feasible when the time step Δt_{Vcr} was applied and corresponding to the critical value consistent with the proper analysis of longitudinal waves, i.e.

$$\Delta t_{Vcr} = \Delta x \sqrt{\frac{\rho}{E}} = 3,044 * 10^{-5} \, [\text{s}]. \tag{14}$$

The critical step had to be evaluated with the formula derived in [10] for the stiff steel rod. The value was derived from this formula:

$$\Delta t_{cr} = \Delta x \sqrt{\frac{m_k}{-P + \dfrac{4EJ}{\Delta x^2}}} = 28,3 \, \mu\text{s}. \tag{15}$$

The condition (15) was derived in reference to the compressive force P the value of which was assumed to be positive. The form (and the form of the formula (14)) required a suitable selection of the spatial step Δx. Given formula (15), the step should satisfy this condition:

$$\Delta x \leq 2 \sqrt{\frac{EJ}{P}} \tag{16}$$

Condition (16) was retained in the adopted discretization of the steel rods in the numerical analyses. The presented numerical results were confirmed by adopting a half-sized division step of the length of the steel rod, which validated the convergence of the results obtained in this work.

The action of a non-decaying shock load caused an avalanche stability loss, albeit after a certain time. This period of time was defined by the slenderness of the steel rod relative to Euler's limit of slenderness. The data presented for the duration indicated that as far as exceptional decaying shock loads are concerned, it would be feasible

to choose their duration of action which, at a specific intensity of the shock loads, would not result in a dynamic stability loss, and be limited to inelastic deformations only. This conclusion constitutes a singularity caused by the inclusion of the effect of the lengthwise axis of the steel rods according to the longitudinal wave behaviour. This effect was not investigated in other research into dynamic instability. There is a theoretical and unnatural schematisation of the lower end support of the steel rods. It provided ideal conditions of reflection of the longitudinal wave, devoid of energy dissipation in the three-dimensional medium of the end support.

REFERENCES

[1] Timoshenko S.P., Gere J.M., *Teoria stateczności sprężystej*, Arkady, Warszawa, 1963.

[2] Gryboś R., *Stateczność konstrukcji pod obciążeniem uderzeniowym*, PWN, Warszawa, 1980.

[3] Kaliski S. i in., *Drgania i fale w ciałach stałych*, Państwowe Wydawnictwo Naukowe, Warszawa, 1966.

[4] Szcześniak Z., *Interaction of longitudinal and transverse vibrations of elastic-plastic bars subjected to eccentric compression*, J. Tech. Phys., 31, 2, 1990, 181-201.

[5] PN-EN1993-1-1**,** *Projektowanie konstrukcji stalowych*, Część 1-1. *Reguły ogólne i reguły dla budynków*.

[6] Biegus A., *Nośność graniczna stalowych konstrukcji prętowych*, PWN, Warszawa, 1997.

[7] Bąk G., Szcześniak Z., *Metoda modelowania dyskretnego procesów falowych w sprężystych warstwowych prętach niepryzmatycznych*, Rozprawy Inżynierskie, 35, 2, IFTR PAS, Warszawa, 1987, 309-325.

[8] Bąk G., Szcześniak Z., *Bezbłędna aproksymacja różnicowa jednowymiarowego problemu falowego w prętach warstwowych*, Biuletyn WAT, nr 12 (412), 1986, 63-74.

[9] Wojewódzki W., *Nośność graniczna konstrukcji prętowych*, Oficyna Wydawnicza Politechniki Warszawskiej, Warszawa, 2012.

[10] Brzuzy A., *Przystosowanie dźwigara kratowego pod działaniem obciążenia impulsowego*, WAT, Warszawa, 2016, rozprawa doktorska.

A. BRZUZY, G. BĄK

Analiza stateczności prętów stalowych poddanych działaniu obciążenia uderzeniowego

Streszczenie. W artykule przedstawiono wyniki analizy numerycznej reakcji sprężysto-plastycznej prętów ściskanych ze wstępną deformacją trwałą ich osi podłużnych pod działaniem wzdłużnego, nieusuwalnego obciążenia uderzeniowego. Rozpatrzono zróżnicowaną intensywność obciążenia do wywołania utraty stateczności włącznie. Wykorzystano metodę różnic skończonych z jawnym schematem całkowania względem czasu równań dynamicznej równowagi. Przyjęto, że czynnikiem inicjującym

niestabilne zachowanie pręta jest ciągła deformacja osi pręta ujmowana zgodnie z aktualnymi procedurami projektowymi. Analizie poddano pręty o zróżnicowanej smukłości, kwalifikowanych, jako wiotkie i krępe. Wykazano, że bardzo duży wpływ na wytężenie prętów i mechanizmy wyboczenia mają efekty falowe wzdłużne. Powodują one szybkozmienne zmiany wartości sił poosiowych oraz istotną koncentrację naprężeń na skutek zjawisk odbicia od nieprzesuwnej podpory. Decyduje to o dyssypacji energii wewnętrznej na odkształceniach plastycznych. Zastosowana metoda rozwiązania umożliwiła oszacowanie wartości dynamicznych sił krytycznych i ich relacji do wartości statycznych.